Desalination and Water Treatment
www.deswater.com

doi: 10.1080/19443994.2013.831785

52 (2014) 7495–7506
December

Taylor & Francis
Taylor & Francis Group

Modeling of permeate flux decline during ultrafiltration of polyvinyl alcohol in a batch cell

Upasna Balyan, Biswajit Sarkar*

University School of Chemical Technology, GGS Indraprastha University, Delhi 110078, India
Tel. +91 11 25302474; email: bsarkr@yahoo.com

Received 12 March 2013; Accepted 15 July 2013

ABSTRACT

Ultrafiltration (UF) of polyvinyl alcohol from aqueous solution is studied in a batch cell over a wide range of operating conditions. The unsteady state nature of the permeate flux decline during UF is caused by changes in the hydraulic boundary condition at the membrane surface due to gel layer formation. An unsteady state mass transfer model is developed for gel-controlled UF in an unstirred cell starting from the basic fluid mechanical analysis of the system. An integral method of solution is used for the solution of the concentration profile in the developing mass transfer boundary layer. The model is used to predict the transient permeate flux decline profile. The transient state behavior in the presence of stirring is estimated by using a model available in literature. The predictions are found to be in good agreement with the experimental flux.

Keywords: Ultrafiltration; Permeate flux; Diffusion; Polyvinyl alcohol; Gel layer

1. Introduction

The textile industry uses synthetic wrap sizing agents in cotton blends such as polyvinyl alcohol (PVA), carboxymethyl cellulose, and various surfactants in the weaving step which helps to smooth and strengthen the fibers. After weaving, the size agents must be washed out with water which produces large volumes of wastewater (about 20% of the total textile wastewater). The wastewater generated in the desizing step contains significant amount of most commonly used sizing agent PVA which is considered to be a prevailing contributor of COD in the textile wastewater. This sizing agent is, however, expensive and nonbiodegradable in nature; thus, it poses challenging waste treatment and/or recovery problems. The concentration of PVA, the major organic component in desizing wastewater, is found to be typically as high as 0.5% [1,2]. Recovery and reuse of valuable and toxic PVA from textile effluent is a major concern in the textile industry from the standpoint of both economics and pollution control. Several techniques have been investigated to reduce the PVA concentrations in the wastewaters to meet stringent environmental legislation. These techniques include electrochemical oxidation [3], advanced oxidation [4], membrane filtration [5–9], etc. Lin and Lan [5] have performed batch experiments to investigate the effects of different types of membrane and operating conditions on the ultrafiltration (UF) performances for the PVA recovery from simulated desizing wastewater. Chen et al. [1] have used nanofiltration membrane on a pilot scale cross flow cell for the treatment of desizing

*Corresponding author.

wastewaters from the bleaching and dyeing industry. Porter [6] has investigated the recovery of PVA from the textile process waste streams using tubular stainless steel membrane, tubular carbon membrane, and spiral wound polyvinyl sulfone membrane. In addition, he has also discussed about the economics and application of automated control to the PVA recovery process. Saleh et al. [7] have investigated the effects of various process parameters on the recovery of PVA from simulated wastewater using polyethersulfone (PES) hollow fiber UF membrane with the molecular weight cut-off (MWCO) 20 kDa with and without addition of carboxymethyl cellulose as synthetic warp sizing agents. About 99% recovery of PVA from synthetic desizing wastewater using bench scale polysulfone hollow fibre membrane (10–30 kDa) has been reported by Lee et al. [8]. Sarkar et al. [9] have used shear enhanced membrane module with inbuilt cleaning facility for the treatment of PVA containing desizing wastewater.

In the light of above brief discussion, it is now accentuated that membrane separations and, in particular, UF are gaining importance for the treatment of desizing wastewater. However, the major drawback of employing UF in the treatment of wastewater containing PVA is the decline in permeate flux during operation i.e., reduction in throughput of the system. This occurs due to concentration polarization i.e., buildup of solute particles over the membrane surface which causes membrane fouling by gel-type layer formation over the membrane surface. Therefore, modeling of UF process is essential for effective design and scale up. It is well known that most of the industrial processes are carried out under cross flow conditions, but batch cell is convenient and is being used extensively for laboratory scale experiments [10,11]. Moreover, the estimated parameters obtained from batch cell seem to be useful for the prediction of the performance of the cross flow experiments in terms of permeate flux [12]. Therefore, study of the filtration under batch mode is essential. However, batch mode experiments under stirring condition are more relevant due to enhancement of permeate flux. Modeling of UF processes in batch cell is generally based on the mass transfer coefficient (k) which is usually derived from the correlations obtained from heat and mass transfer analogies for nonporous conduit [13,11]. However, mass transfer coefficient for a batch cell is generally empirical in nature. Hence, the use of standard correlation leads to an inaccurate estimation of the mass transfer coefficient and hence incorrect prediction of flux decline. One way to avoid this is to solve the convective-diffusive solute mass balance equations with pertinent boundary conditions. Shen and Probstein [14] have first presented a model for unstirred batch UF and solved the governing convective-diffusive equation numerically. Analytical solution of the governing convective-diffusive equation using integral method is reported by Trettin and Doshi [15]. Gel layer controlled filtration is very common in membrane processes. This occurs in case of filtration of many gel-forming solutes such as pectin, PVA, etc. The modeling of unstirred batch system for quantification of flux decline is outlined by Chudacek and Fane [16] using gel-filtration theory. However, theoretical model for the unstirred batch cell under the framework of boundary layer theory for gel-controlled UF is very scant in literature. Therefore, a model having more fundamental basis is essential to quantify flux decline during gel-controlled UF. In the present study, transient flux decline profile is modeled from the first principles in an unstirred batch cell under concentration mode considering resistance-in-series model based on gel layer theory. The model includes the developing mass transfer boundary layer over the gel layer, which is the most realistic situation. Thus, this model overcomes the shortcoming of conventional film theory [17] that considers a constant mass transfer boundary layer thickness. In the proposed model, specific gel-layer resistance is the only parameter that needs to be optimized using experimental data. In a batch UF, the solute concentration varies with operation time. The developed model takes into account the variation of bulk concentration and bulk volume with the time of operation during batch mode of operation. The proposed model is used to quantify the transient flux decline as well as volume reduction factor (VRF) during batch concentration mode of operation. The model is successfully applied for the UF of aqueous solution of PVA over a wide range of operating conditions. The transient flux profile in the presence of stirring is predicted using the model developed in our previous study [18].

2. Theory

The models available in literature for quantification of flux decline in case of gel-layer controlled UF for unstirred cell are mostly derived from the filtration theory [16,19]. In this case, bulk concentration is assumed to be constant. However, the variation of solute concentration with operation time is an important factor which affects the permeate flux. In the following section, a model is developed from the first principles including the variation of solute concentration with time for the prediction of transient flux decline as well as the VRF.

The aqueous solution of PVA to be filtrated is charged in the batch cell and then pressurized over the membrane surface to facilitate the water to pass through the membrane. For fully retentive membrane ($C_p = 0$), the solute mass balance in the cell results in the following equation in dimensionless form as [18],

$$\frac{dC_b^*}{d\tau} = \frac{Pe_w(\tau)\ v\ C_b^*}{V_f^*} \quad (1)$$

where $C_b^* = \frac{C_b}{C_0}$; $\tau = \frac{tD}{R^2}$; $v = \frac{AR}{V_0}$; $Pe_w = \frac{V_w R}{D}$, $V_f^* = \frac{V_f}{V_0}$.

The solution retained within the pores of the accumulating gel volume on the membrane surface is assumed to be negligible. The variation of retentate volume with time can be obtained by writing the material balance in the cell and can be expressed in dimensionless form as [18],

$$\frac{dV_f^*}{d\tau} = -Pe_w(\tau)v \quad (2)$$

The two-dimensional unsteady state solute mass balance equation within the mass transfer boundary layer is written as,

$$\frac{\partial C}{\partial t} + v_r\frac{\partial C}{\partial r} + v_y\frac{\partial C}{\partial y} = D\frac{\partial^2 C}{\partial y^2} \quad (3)$$

where C is the concentration of solute, v_r and v_y are velocity components in the radial and axial directions, respectively. D is the solute diffusivity (assumed as constant). r and y are radial and axial coordinates, respectively. The permeate flux is a function of radius of the cell. The incorporation of the variation of permeate flux with radial position at a given time makes the analysis complex and for the sake of simplicity, the variation of solute concentration with radial position is neglected. Assuming one-dimensional flow normal to the membrane surface, Eq. (3) is simplified and can be written in dimensionless form as

$$\frac{\partial C^*}{\partial \tau} - Pe_w\frac{\partial C^*}{\partial y^*} = \frac{\partial^2 C^*}{\partial y^{*2}} \quad (4)$$

The Eq. (4) has the following initial and boundary conditions,

$$\text{At} \quad \tau = 0,\ C^* = 1 \quad (5)$$

$$y^* = L^* + \delta_c^*,\ C^* = C_b^* \quad (6)$$

The liquid height in the cell (order of magnitude of 10^{-2} m) is generally 4–5 order magnitude higher compared to concentration boundary layer thickness (order of magnitude of 10^{-6} m). Since the concentration boundary layer thickness is extremely small, most part of the channel is outside of the mass transfer boundary layer. Thus, the boundary condition (Eq. (6)) used for the solution of Eq. (4) is valid at the edge of the boundary layer. The gel-layer formation over the membrane surface depends on the rate of solute migration towards the membrane due to convection and the rate at which the solutes migrate away from the membrane due to back diffusion. This leads to following boundary condition at the gel–solution interface,

$$\text{At} \quad y^* = L^*,\ \frac{\partial C^*}{\partial y^*} + Pe_w C_g^* = \rho_g^*\frac{dL^*}{d\tau} \quad (7)$$

The diffusion coefficient is calculated using the Stokes-Einstein equation as,

$$D = \frac{KT}{3\pi\mu_b d_p} \quad (8)$$

where K, T, μ, and d_p are the Boltzmann constant, absolute temperature, viscosity of the solution, and equivalent spherical diameter of the particle, respectively. The average diameter of the gel-forming PVA molecule is estimated assuming spherical molecule and using the following relationship [20].

$$M_\omega = z d_p^3 \quad (9)$$

where M_ω is the average molecular weight of gel forming material, the value of z is taken as 6×10^{29} gm/gm-mole m^3 [20]. The corresponding value of equivalent spherical diameter of PVA is found to be 5.93×10^{-9} m. For estimation of gel-layer concentration of PVA, experiments are carried out under steady state in the cross flow cell, using various feed concentrations. The steady state permeate flux can be expressed as,

$$V_{w,CF}^{ss} = k\ \ln\frac{C_g}{C_0} \quad (10)$$

where k is the mass transfer coefficient; C_0 and C_g are feed and gel concentration of PVA, respectively. Thus, the variation of the steady state permeate flux with feed concentration is a straight line in semi-log plot. The straight line variation can be extrapolated in order to obtain the gel-layer concentration [21]. Eq. (4) is simplified using the integral approach, the following concentration profile within the thin concentration boundary layer is assumed:

$$C^* = \frac{C}{C_0} = a_1 + a_2\left(\frac{y^*}{\delta c^*}\right) + a_3\left(\frac{y^*}{\delta_c^*}\right)^2 \quad (11)$$

where $\delta_c^* = \frac{\delta_c}{R}$; $L^* = \frac{L}{R}$.

Eq. (11) satisfies the following boundary conditions:

$$\text{at} \quad y = \delta_c^*,\ C^* = C_b^* \quad (12)$$

$$\text{at} \quad y^* = \delta_c^*,\ \frac{\partial C^*}{\partial y^*} = 0 \quad (13)$$

$$\text{at} \quad y^* = L^*,\ C^* = \frac{C_g}{C_0} = C_g^* \quad (14)$$

where C_g is the gel concentration of solute. With the help of the above boundary conditions, Eq. (11) can be written as,

$$C^* = C_g^* - 2\left(C_g^* - C_b^*\right)\left(\frac{y^*}{\delta_c^*}\right) + \left(C_g^* - C_b^*\right)\left(\frac{y^*}{\delta c^*}\right)^2 \quad (15)$$

Substituting the partial derivative of C^* with respect to y^* and τ from Eq. (15) into the nondimensional governing equation (Eq. (4)), the following equation is obtained

$$\frac{2y^*}{\delta_c^{*2}}(C_g^* - C_b^*)\left(1 - \frac{y^*}{\delta_c^*}\right)\frac{d\delta_c^*}{d\tau} + \frac{dC_b^*}{d\tau}\left(\frac{2y^*}{\delta_c^*} - \frac{y^{*2}}{\delta_c^{*2}}\right) + \frac{2}{\delta_c^*}\mathrm{Pe_w}(C_g^* - C_b^*)\left(1 - \frac{y^*}{\delta_c^*}\right) = \frac{2}{\delta_c^{*2}}(C_g^* - C_b^*) \quad (16)$$

Multiplying both sides of the Eq. (16) by dy^* (taking zeroth moment) and then integrating across the boundary layer thickness, i.e. from 0 to δ_c^*, the following expression is obtained:

$$\frac{\left(C_g^* - C_b^*\right)}{3}\frac{d\delta_c^*}{d\tau} + \frac{2}{3}\delta_c^*\frac{dC_b^*}{d\tau} + \mathrm{Pe_w}\left(C_g^* - C_b^*\right) = \frac{2}{\delta_c^*}\left(C_g^* - C_b^*\right) \quad (17)$$

Substituting Eq. (1) into Eq. (17) and after simplification, the following expression is obtained:

$$\frac{d\delta_c^*}{d\tau} = \left(\frac{3}{(C_g^* - C_b^*)}\right) \times \left[\frac{2(C_g^* - C_b^*)}{\delta_c^*} - \frac{2}{3}\mathrm{Pe_w}\delta_c^*\frac{C_b^*}{V_f^*}v - \mathrm{Pe_w}(C_g^* - C_b^*)\right] \quad (18)$$

Following equation is obtained by substituting the partial derivative of C^* with respect to y^* from Eq. (15) into the Eq. (7).

$$\frac{dL^*}{d\tau} = \frac{1}{\rho_g^*}\left[\mathrm{Pe_w}C_g^* - \frac{2(C_g^* - C_b^*)}{\delta_c^*}\right] \quad (19)$$

The permeate flux during the gel-layer controlled UF is expressed by a resistance in series formulation including the flow resistance due to the membrane itself and the deposited gel layer over the membrane surface. The permeate flux at any time may be expressed in dimensionless form as [18],

$$\mathrm{Pe_w}(\tau) = \frac{\mathrm{Pe_w^0}}{(1 + R_g^*(\tau))} \quad (20)$$

where $\mathrm{Pe_w^0} = \frac{\Delta P R}{\mu_p R_m D}$, $R_g^* = aL^*$, $a = \frac{\alpha' R}{R_m}$, and $\alpha' = 180\frac{(1-\varepsilon_g)^2}{\varepsilon_g^3 d_p^2}$.

In order to solve the Eq. (18), one initial condition is required and the obvious initial condition is at $\tau = 0$, $\delta_c^* = 0$. But, this condition renders Eq. (18) indeterminate. Therefore, an asymptotic solution has been sought to the limit, $\tau \to 0$. As $\tau \to 0$, $c_b^* \to 1$, $\delta_c^* \to 0$ under this condition, Eq. (18) becomes

$$\frac{d\delta_c^*}{d\tau} = \frac{6}{\delta_c^*} \quad (21)$$

The solution of the above equation is

$$\delta_c^* = \sqrt{12\tau} \quad (22)$$

A very small value of τ is chosen (10^{-10}) as required for the stability of the solution and the corresponding starting value of δ_c^* is evaluated by Eq. (22). Thereafter, the solution is performed for the whole duration of experiment. For a given set of operating conditions, the governing ordinary coupled differential and algebraic equations Eqs. (1), (2), (18), (19), and (20) are solved using fourth-order Runge–Kutta method. The specific gel-layer resistance (α) is obtained by optimizing the experimental flux with the model-calculated values. It needs to be pointed out that the values of the specific gel resistance cannot be calculated a priori, and the porosity ε_g can be a

function of the operating conditions (e.g. transmembrane pressure).

2.1. For stirred cell

The time variation of the growth of the gel layer thickness can be written in terms of dimensionless form as [18]:

$$\rho_g^* \frac{dL^*}{d\tau} = \left[\frac{C_g^* - C_b^* \exp\left(\frac{Pe_w}{Sh}\right)}{1 - \exp\left(\frac{Pe_w}{Sh}\right)}\right] Pe_w \quad (23)$$

where $L^* = \frac{L}{R}$.

The following Sherwood number relationship [22] was used in the stirred cell.

$$Sh = \frac{kR}{D} = 0.285 \quad Re^{0.55} \quad Sc_b^{0.35} \left(\frac{\mu_b}{\mu_g}\right)^{0.14} \quad (24)$$

$Re < 32,000$

$$Re = \frac{\rho_b \omega R^2}{\mu_b}; \; Sc_b = \frac{\mu_b}{\rho_b D} \quad (25)$$

Followings are the sequence of steps for calculation of permeate flux, gel layer thickness, and VRF as outlined below:

(1) For known input parameters of operating conditions, membrane parameter and physical properties such as ΔP, C_0, R_m, A, V_0, R, C_g, μ, d_p, and ρ_g, a value of specific gel-layer resistance (α) is guessed.

(2a) For unstirred cell, assuming bulk diffusivity is not a function of concentration, v_w^{cal} is calculated by solving the coupled differential and algebraic equations, Eqs. (1), (2), (18), (19), (20), and (22) with the following initial condition, at $\tau = 10^{-10}$, $L* = 0$, $C_b^* = 1$, and $V_f^* = 1$.

(2b) For stirred cell, v_w^{cal} is calculated by solving the coupled differential and algebraic equations, Eqs. (1), (2), (20), (23) and (24) with the following initial condition, at $\tau = 0$, $L* = 0$, $C_b^* = 1$, and $V_f^* = 1$.

(3) The time, τ, is increased to $\tau + \Delta\tau$ next.

(4) Steps 2 to 3 are repeated till $\tau = \tau_{total}$

(5) If $\sum_{i=1}^{N_{total}} \left(\frac{V_w^{exp} - V_w^{cal}}{V_w^{exp}}\right)^2 \leq 0.001$ the program is terminated and transient profiles of permeate flux is obtained. The corresponding value of α is recorded. If not, another value of α is guessed in Step 1 and the process is continued till the given convergence is achieved. The profiles of permeate flux, gel-layer thickness, gel-layer resistance, and VRF for both stirred as well as unstirred condition are obtained as a function of time.

3. Materials and methods

3.1. Materials

Analytical grade PVA of average molecular weight 1,25,000 was procured from M/s, Merck India Ltd., Mumbai, India, and PES membrane of MWCO 30 kDa, obtained from M/S. Permionics, Boroda (India), were used for the experiment.

3.2. Operating conditions

Filtration experiments were conducted taking into account the effect of the three major conditions i.e., stirrer speed, transmembrane pressure, and feed concentration on the transient flux decline. One parameter was varied while the others were held constant to get an exact picture of the dependence. The effect of transmembrane pressures on permeate flux was investigated in the UF regime as 207, 345, 483, and 690 kPa. The stirrer speeds were chosen such that the effect of stirring on system performance can be observed while maintaining laminar flow regime during UF. Four stirring speeds, 800, 1,000, 1,200, and 1,400 rpm, were used. The corresponding values of Reynolds number are 15,166, 18,955, 22,755, and 26,544, respectively. The Reynolds number for all the operating range of stirrer speed from 800 to 1,400 rpm is less than 32,000; that is, the hydrodynamic flow condition is in the laminar range [23]. In desizing wastewater, the typical concentration of PVA was found to be as high as 5 kg/m^3 [1,2]. Therefore, in the present investigation, the PVA concentrations in the feed were selected as 1, 3, 5, and 8 kg/m^3. The pH of the PVA solution was kept constant at 7.0 in the present study as pH of desizing wastewater was reported to be about 7.0 [8]. The pH of the PVA solution was adjusted by dropwise addition of 10 mM NaOH and HCl. A total of 26 experiments were performed including both stirred and unstirred conditions and subsequently experimental data were used for comparison with the theoretical model predicted results. For estimation of PVA gel concentration, cross flow experiments were conducted selecting PVA concentrations in the feed as 1, 10, 20, 30, and 40 kg/m^3. Other operating conditions such as pH, transmembrane pressure, and cross flow velocity were fixed at 7.0, 552 kPa and 0.09 m/s, respectively. Physical properties of aqueous solution of PVA are given in Appendix.

3.3. Experimental setup and experimental procedure

Two different experimental setups were used in the present study. A batch (stirred and unstirred) cell was used under the batch concentration mode to observe the effects of the various operating conditions

on permeate flux decline. A cross flow cell was used to obtain the gel concentration of PVA.

3.3.1. Batch cell experiment

A batch cell made of stainless steel was used for the UF experiments. The cell consisted of three detachable parts. The top flanged section was with the stirring arrangement; the middle part was the short cylindrical shell; and the lower part was a grooved base where the porous stainless steel support and the membrane were placed. The inner diameter of the cell was 0.076 m and the effective filtration area of the circular membrane was $32.15 \times 10^{-4}\,m^2$. The feed chamber was connected to a nitrogen cylinder to generate pressure in the cell. The stirrer at the top of the cell was externally attached to a motor through a belt. A voltage control device was used to control the speed of stirrer and it was measured by a hand-held digital tachometer (Scientific International, Delhi, India). The schematic of the experimental setup is shown in elsewhere (18). The membrane used in the experiments was a PES membrane of MWCO 30 kDa. The membrane was initially compacted at a pressure of 828 kPa (higher than the maximum operating pressure used in this study, i.e., 690 kPa) for 3 h using distilled water. The membrane permeability was found to be 8.0×10^{-11} m/Pa s. After the water run, the cell was charged with 500 mL of the feed solution and was pressurized at the operating pressure using a pressure regulator and a nitrogen cylinder. It is very difficult to measure the permeate flux along the radial position of the cell at a particular time. Hence, the radial average permeate flux is measured for different time of operation. During each experiment, cumulative volume of permeate from different radial position of the cell was collected in a measuring cylinder as a function of time through a common outlet from the bottom of the cell. From the slope of the cumulative volume–time plot, the radial average permeate flux as a function of time was obtained. The duration of each experiment was about 60 min. All experiments were conducted at 25 ± 2°C. Each experiment is repeated three times. All the experiments show repeatability to within ±3% in terms of flux measurement. However, it may be noted here that since the experiments were conducted under batch mode, the permeate stream was continuously taken out resulting in an increase in solute concentration accompanied by a reduction in feed volume with time of operation.

3.3.2. Cross flow cell experiment

The schematic of the continuous cross flow UF unit similar type is shown elsewhere [24]. The feed tank of 10 L. capacity was connected to a single cylinder reciprocating pump. From the feed tank, feed solution is pumped and allowed to flow tangentially over the membrane surface through a thin channel of 38 cm in length, 6 cm in width and 4.7 mm in height. Inside the rectangular channel, the membrane is placed on a stainless steel porous support. The retentate is recycled to the feed tank. A rotameter in the retentate line measures the flow rate. Pressure inside the UF cell is maintained by operating the bypass valve and is measured by a pressure gauge. Permeate is collected from bottom of the cell. The permeate was collected from the bottom outlet of the cell and it was recycled to the feed tank to make the feed concentration constant. The effective filtration area is $228\,cm^2$.

3.3.3. Membrane cleaning protocol

At the end of each experiment, the membrane module was dismantled and the membrane was taken out and thoroughly washed with distilled water at room temperature 25 ± 2°C, followed by 45 min of static surfactant washing using sodium dodecyl sulfate and finally membrane was washed with distilled water. After such thorough washing, the cell was reassembled and the membrane permeability was again measured using distilled water. This procedure was allowed for recovery of the pure initial water flux within 95%. After this, the membrane cell was ready for the next experiment. Freshly prepared PVA feed was used for each experiment.

3.4. Analysis of the feed and permeate

PVA concentration in feed as well as permeate was measured with a refractometer (Model DR 301-95, A.Kruss Optronic, Germany). PVA content in the permeate of all the experiments under present investigation was found to be nil. Viscosity of the samples was measured by Ostwald viscometer. Density of feed solution and permeate was measured by Density meter (Mettler Toledo, USA). pH of the feed solution was determined by pH meter (M/S Accumax India).

4. Results and discussion

4.1. Estimation of gel concentration of PVA

For estimation of the gel-layer concentration, experiments were carried out under steady state in the cross flow cell at various feed concentrations and

cross flow velocities for a fixed transmembrane pressure. Fig. 1 represents the variation of steady state permeate flux as a function of feed concentration for different values of cross flow velocity. It is observed from the figure that the gel-layer concentration is about 65 kg/m^3 by extrapolating the straight line variation. It is further noticed that gel concentration is almost independent of cross flow velocity. It may be noted here that the viscosity corresponding to gel concentration is extrapolated from Eq. (A1), and the value is found to be 29×10^{-3} Pa s.

4.2. Analysis of model predictions and comparison with experimental observation

The profiles of permeate flux and gel-layer thickness for different feed solute concentrations for fixed value transmembrane pressure in the unstirred and stirred batch cell have been shown in Figs. 2(a) and (b), respectively. The symbols are the experimental data and solid lines are the model predictions. Experimental flux values show repeatability to within ± 3% and are shown in these figures with error bar. The concentration boundary layer profile for different feed solute concentrations is shown in the inset of the Fig. 2(a). For a fixed feed concentration, boundary layer thickness increases rapidly with time initially and gradually thereafter. Moreover, for higher feed concentrations, concentration boundary layer thickness is more at fixed time. The value of specific gel-layer resistance (α) is evaluated by minimizing the sum of the least squares between the experimental and the calculated flux decline data. The value of α is estimated as $(11.22 \pm 0.5) \times 10^{15}$ m/kg. It is observed that

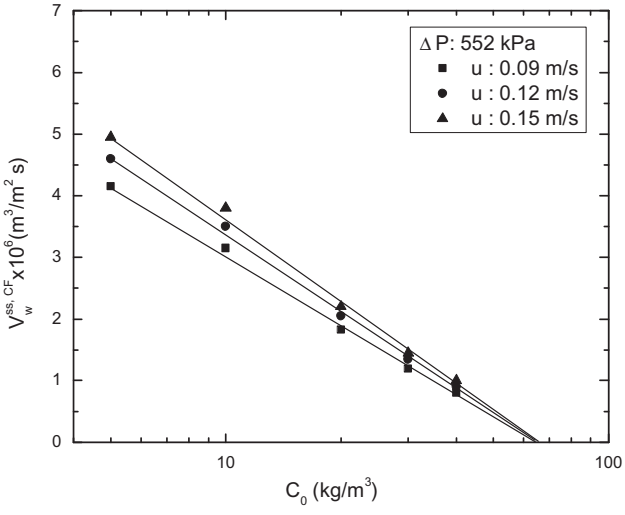

Fig. 1. Estimation of gel layer concentration of PVA.

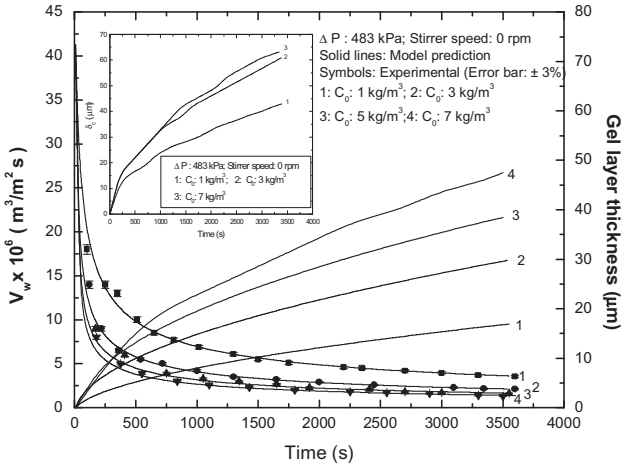

Fig. 2(a). Variation of permeate flux and gel layer thickness with time at different feed concentrations in absence of stirring.

model predictions are within ± 5% to the experimental results. The value of specific gel-layer resistance is found to be unaltered with changing the feed concentration. Similar trends are observed in both stirred and unstirred conditions. The sharp decline in permeate flux observed at the beginning of filtration can be attributed to the rapid development of concentration polarization on the fully retentive membrane surface as observed in the inset of the Fig. 2(a). As the time of operation progresses, there is more accumulation of solutes over the membrane surface leading to severe concentration polarization. The slower flux decline at later stages can be attributed to the formation of gel layer on the membrane surface. This is a direct consequence of the rapidly growing gel-layer thickness over the membrane surface at the beginning of filtration and gel layer growth is gradual as the time progresses. It is further noticed that with increase in solute feed concentration, concentration polarization increases as evident from the inset of the Fig. 2(a) resulting in an increase in gel-layer thickness over the membrane surface. It is further noticed that an increase in flux is observed with decrease in feed concentration keeping other operating conditions unchanged. With increase in PVA feed concentration, concentration polarization increases resulting in an increase in gel-layer thickness over the membrane surface. This leads to decrease in permeate flux with thicker gel layers. For example, in the absence of stirring (Fig. 2(a)), at the end of the operation, with an increase in feed concentration from 1 to 7 kg/m^3, for a fixed pressure (483 kPa), the permeate flux decreases from 3.6×10^{-6} m^3/m^2 s to 1.4×10^{-6} m^3/m^2 s. The concentration boundary layer thickness and gel-layer

thickness increases from 43 to 62.7 μm and from 16.9 to 45.6 μm, respectively, for the same increment of feed concentration keeping other operating condition unchanged. However, in the presence of stirring (Fig. 2(b)), for the same increase in feed concentration, for a fixed stirrer speed (1,000 rpm) and pressure (483 kPa), the permeate flux decreases from $8.2 \times 10^{-6}\,m^3/m^2\,s$ to $3.1 \times 10^{-6}\,m^3/m^2\,s$ and gel layer thickness increase from 6.5 to 20.25 μm.

Fig. 3 shows the variations of VRF with time for different feed concentration. VRF is defined as the ratio of initial feed volume to the retentate volume at any time of filtration. Since the retentate volume decreases continuously with the progress of the filtration as permeate is taken out without recycle, VRF continues to increase with time as also observed in Fig. 3. This is true for all PVA feed concentration. It is also noticed that at any particular time of filtration, the VRF is less for higher PVA feed concentration for a fixed transmembrane pressure. This may be explained by the fact that at higher PVA feed concentration, the concentration polarization is more severe leading to an increased gel-layer thickness over the membrane surface. This results to a decrease in permeate flux. Therefore, VRF decreases with increase in PVA feed concentration. For example, at the end of the operation, with an increase in PVA feed concentration from 1 to 7 kg/m^3 for a fixed pressure (483 kPa), VRF decreases from 1.18 to 1.06 (i.e., about 11%). Furthermore, one can see that the effect of pressure on the VRF profile is negligible by comparing the curves 2 and 4.

The profiles of dimensionless gel-layer resistance with time at various feed concentrations in absence of stirring and in presence of stirring are shown in Figs. 4 (a) and (b), respectively. From the figure, it is evident that for a fixed feed concentration, gel-layer resistance increases steeply with time initially and gradually thereafter. It is also evident from the figures that in both stirred and unstirred conditions, gel-layer resistance increases with increase in feed concentration at a particular time of operation. The concentration polarization increases with increase in feed concentration, resulting in higher gel-layer thickness and thereby, increasing the value of gel layer resistance. For example, in the absence of stirring (Fig. 4(a)), at the end of the operation, with an increase in feed concentration from 1 to 7 kg/m^3, for a fixed transmembrane pressure drop (483 kPa), dimensionless gel-layer resistance increases from 10.4 to 28.6. However, in the presence of stirring (Fig. 4(b)), for the same increase in feed concentration, dimensionless gel resistance increases from 4.0 to 12.46. It is also noticed from Fig. 4(a) that with increase in pressure, gel-layer resistance increases keeping other operating conditions unchanged. This is simply because at higher transmembrane pressure, more solutes are convected toward the membrane surface resulting in higher gel-layer thickness and thereby, increasing the value of gel-layer resistance. For example, in absence of stirring (Fig. 4(a)), at the end of the operation, with an increase in pressure from 483 to 690 kPa for a fixed feed concentration (3 kg/m^3), gel-layer resistance increase from 18.3 to 24.9.

Fig. 5 illustrates the transient behavior of permeate flux and growth of gel-layer thickness with time at different operating transmembrane pressure for fixed values of feed concentration. The symbols are the

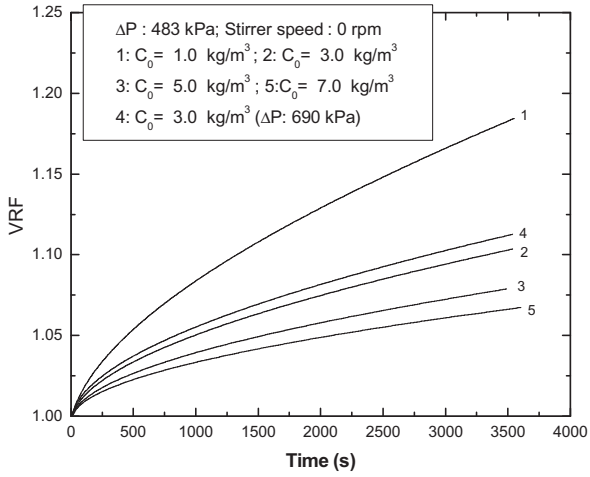

Fig. 3. Variation of VRF with time for different feed concentration.

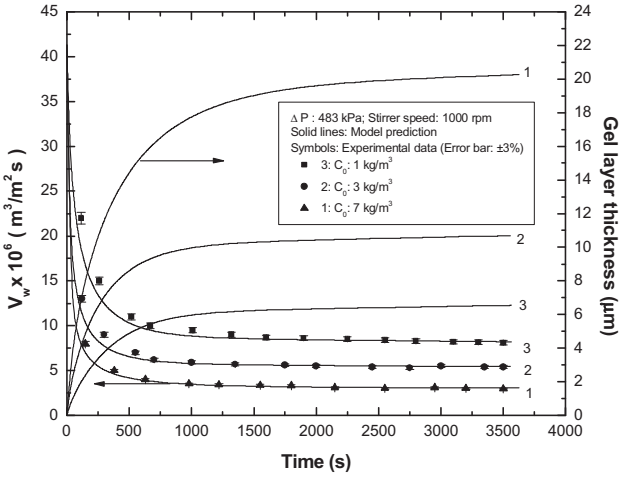

Fig. 2(b). Variation of permeate flux and gel layer thickness with time at different feed concentrations in presence of stirring.

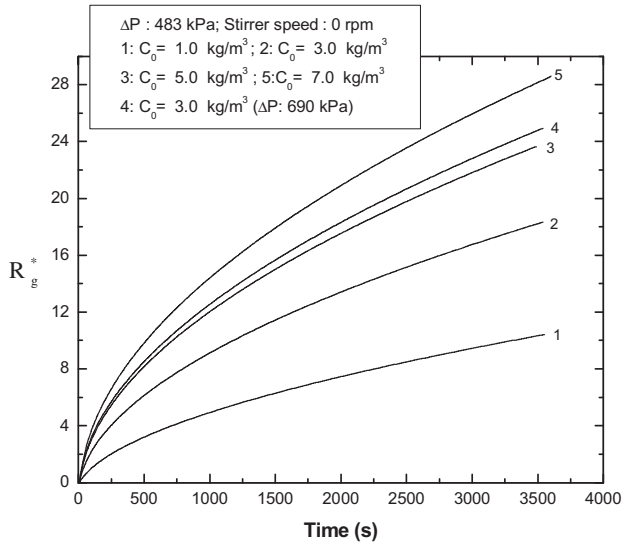

Fig. 4(a). Variation of dimensionless gel layer resistance with time for different feed concentration in absence of stirring.

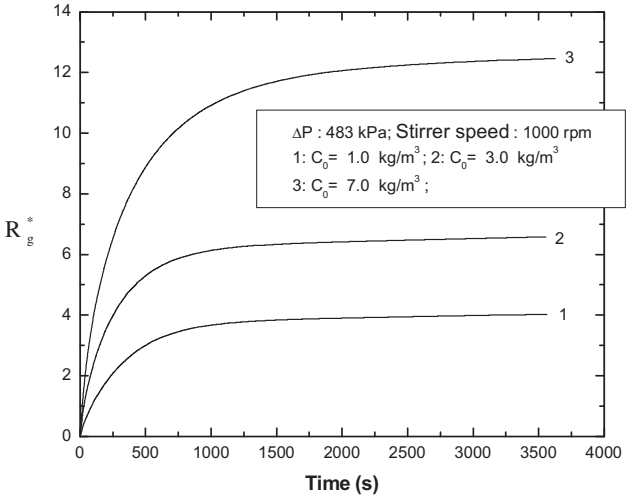

Fig. 4(b). Variation of dimensionless gel layer resistance with time for different feed concentration in presence of stirring.

experimental data and solid lines are the model predictions. The value of specific gel-layer resistance (α) is generally evaluated by minimizing the sum of the least squares between the experimental and the calculated flux decline data. For a gel forming solute, the specific gel-layer resistance, α, varies with transmembrane pressure which is observed in the present study as well as other studies [10,22]. It is evident from the present study that the value of α increases with increase in transmembrane pressure as it causes compaction of the gel layer which facilitates further

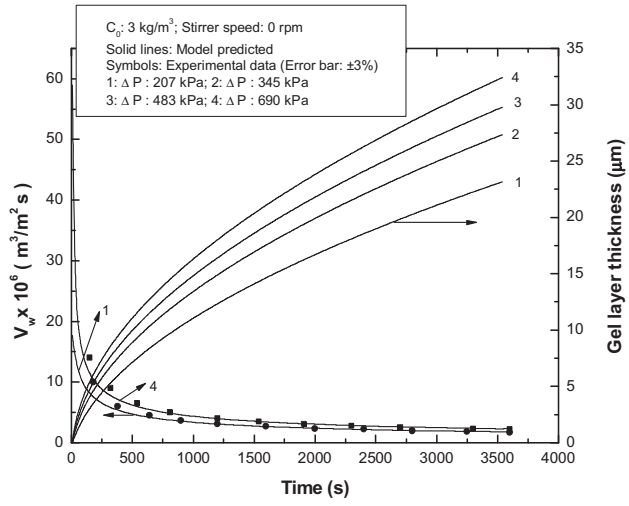

Fig. 5. Variation of permeate flux and gel layer thickness with time at different transmembrane pressure in absence of stirring.

growth of the layer. Gel compressibility appears in the definition of gel-layer resistance, $R_g = \alpha' L$ (Eq. (29)). Where, the parameter α' consists of specific gel resistance (α), gel porosity (ε_g), particle diameter, and gel density (ρ_g). L is the gel-layer thickness. Out of these parameters, gel density is the intrinsic property of the gel layer, independent of the operating conditions. Specific gel-layer resistance and gel porosity are pressure dependent. At a constant pressure, specific gel-layer resistance and porosity are also constant. Thus, these parameters are considered to be constant and invariant with operating time. The expression for the prediction of permeate flux in case of gel layer controlled UF for unstirred cell is available in literature [16]. The specific gel-layer resistance of PVA gel can also be obtained by fitting our experimental flux data to the model expression proposed by Chudacek et al. [16], $(1/V_w^2 = 1/V_{w,0}^2 + \alpha\varphi t$, where, $\varphi = 2\mu C_0/\Delta P$ is constant for a given pressure. The slope of $1/V_w^2$ vs. time curve for a given operating conditions, namely, ΔP and C_0 gives the value of specific gel resistance. The evaluated values of specific gel resistance (α) are correlated with operating transmembrane pressure by a simple relation as $\alpha = \alpha_0(\Delta P)^n$ where n and α_0 are the gel compressibility index and coefficient, respectively. Transmembrane pressure (ΔP) is in kPa. For compressible gel, n is less than 1 and it is 1 for incompressible gel layer. In the present model, the values of α_0 and n are found to be 6.6×10^{14} m/kg and 0.459, respectively, with the correlation coefficient 0.998, whereas using the flux expression proposed by Chudacek et al. [16], the values of α_0 and n are found to be 6.4×10^{14} m/kg and 0.423, respectively, with the

correlation coefficient 0.99. Thus, the optimized values obtained from both the modes are found to be in the same order of magnitude. It can also be observed from both the models that gel layer behaves like a compressible one within the range of operating transmembrane pressure under investigation. Gel porosity (ε_g) can be calculated using Kozeny–Carman equation [10], where, $\alpha = 180(1-\varepsilon_g)/\varepsilon_g^3 d_p^2 \rho_g$. The evaluated values of α and ε_g for different operating pressures obtained from both the modes are presented in Table 1. It is observed from the Table 1 that the gel porosity decreases from 0.57 to 0.50 with increase in operating pressure from 207 to 690 kPa. It can be observed from the figure that gel-layer thickness increases with increase in operating transmembrane pressure for a fixed feed concentration. As explained earlier, increased pressure facilitates convective flux toward the membrane resulting in higher rates of solute accumulation near the membrane surface leading to more severe concentration polarization. This would result in thicker gel layers at higher pressure. For example, at the end of the operation, with an increase in pressure from 207 to 690 kPa for a fixed feed concentration (3 kg/m^3), gel-layer thickness increase from 23.15 μm to 32.4 μm However, at the end of the operation, no significant change in permeate flux is observed with increase in pressure. This is because due to increase in pressure, the enhanced driving force for solvent flux is almost fully compensated by the resistance offered by the growing gel layer on the membrane surface and/or due to compaction of the gel layer. The pressure-independent permeate flux is a strong indication of gel-controlled UF.

Fig. 6 describes the variation of permeate flux and gel-layer thickness with time for different stirring speed for a PVA feed concentration of 5 kg/m^3 and transmembrane pressure of 483 kPa. The symbols are the experimental data and solid lines are the model predictions. This figure shows a good agreement with calculated profiles and the experimental data (±5%). It is noticed that the value of specific gel-layer resistance

Table 1
Optimized values of specific gel layer resistance α and gel porosity ε_g of PVA gel for different operating pressures

ΔP (kPa)	$\alpha \times 10^{-15}$ (m/kg) (present model)	ε	$\alpha \times 10^{-15}$ (m/kg) [Chudacek et al. 16]	ε_g
207	7.6	0.57	6.3	0.60
345	9.6	0.54	7.5	0.58
483	11.2	0.53	8.5	0.56
621	12.6	0.50	10.0	0.54

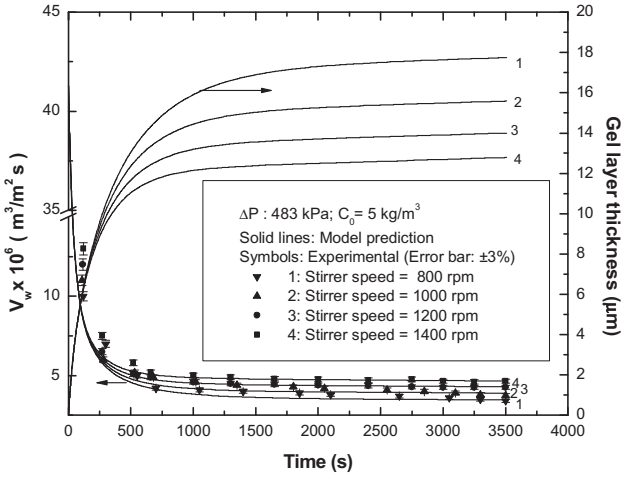

Fig. 6. Variation of permeate flux and growth of gel layer thickness with time for different stirrer speed.

(α) is not affected with change in stirring speed. It may also be observed that experimental results deviate from model prediction during the initial period. This behavior can be the consequence of the combination of two reasons; first, experimental error margin involved in initial permeate flux data is high as the system takes some time to stabilize; second, the model is assumed to be a true gel-controlled UF from the beginning of the operation. However, in all stirring condition, long-term flux decline data (which is more important from a practical point of view) is predicted with high accuracy. At a fixed operating pressure and PVA feed concentration, with increase in stirrer speed, the permeate flux increases with reduction of gel-layer thickness. The sharp initial drop in permeate flux at the beginning of the operation can be attributed to the sudden formation of concentration polarization layer. As the time of filtration progresses, there is more build up of solutes over the membrane surface leading to severe concentration polarization. The smoother and slower flux decline at later stages can be attributed to gel-layer formation on the membrane surface. As stirring speed increases, the concentration polarization decreases due to enhanced turbulence close to the membrane surface, leading to an increase mass transfer coefficient and, therefore, growth of the gel layer is restricted due to more forced convection. This leads to decrease in gel-layer thickness with increase in permeate flux as observed from the figure. For example, at the end of the operation, for transmembrane pressure of 483 kPa and PVA feed concentration of 5 kg/m^3, as the stirrer speed increases from 800 to 1,400 rpm, permeate flux increases from 3.45×10^{-6} m^3/m^2 s to

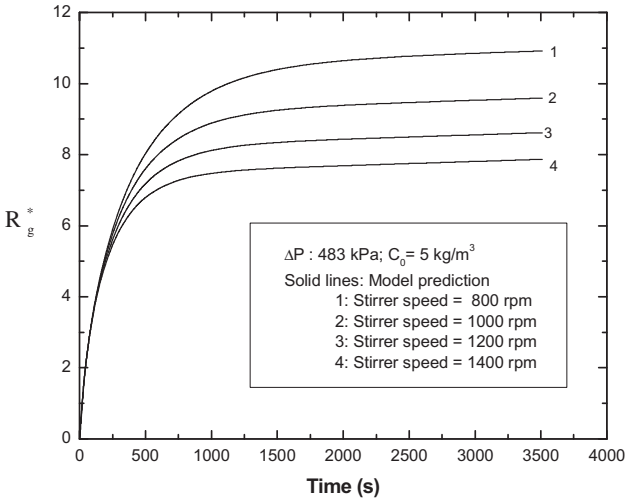

Fig. 7. Variation of dimensionless gel layer resistance with time for different stirrer speed.

4.65×10^{-6} m^3/m^2 s and gel-layer thickness decreases from 17.75 to 12.8 μm.

Development of dimensionless gel-layer resistance as a function of time for different stirring speed for a PVA concentration of 5 kg/m^3 and transmembrane pressure of 483 kPa is shown in Fig. 7. As discussed earlier, the reduction of gel-layer thickness is a direct result of enhancement of turbulence in the flow channel that increases the backward diffusion of solutes from the gel layer to the bulk resulting in decrease in concentration polarization over the gel layer. This restricts the formation and growth of gel layer on the membrane surface, leading to an increase in permeate flux. Since the gel-layer characteristics remain unaltered, the gel-layer resistance is proportional to gel-layer thickness. Hence, the gel-layer resistance varies with the operating conditions similar to gel-layer thickness. Thus, gel-layer resistance decreases with stirring speed. It is observed from this figure that at the end of filtration, for transmembrane pressure of 483 kPa and PVA feed concentration of 5 kg/m^3, the value of gel-layer resistance lies between 7.9 to about 10.9 times of membrane resistance in the range of stirring speed considered herein.

5. Conclusions

A theoretical model based on integral method assuming suitable concentration profile in the mass transfer boundary layer is presented in this paper. The effects of different process parameters such as feed concentration, transmembrane pressure, and stirring speed on permeate flux are investigated during UF of PVA from aqueous solution using a 30 kDa flat sheet PES membrane in a batch cell. The parametric studies conducted are consistent with the basic understanding of the process. The proposed model is used to predict the transient permeate flux decline and growth of gel-layer deposition. The present model requires a parameter, the specific gel-layer resistance, which is estimated by optimizing the experimental transient flux decline profile. The estimated values of specific gel-layer resistance are in the same order of magnitude as optimized by other model available in the literature under various operating conditions studied herein. The predicted flux values using this optimized parameter are successfully compared with the experimental results under a wide range of operating conditions, confirming the increase of permeate flux with increase in stirring speed and with decrease in feed concentration. This proposed model which is validated using experimental data is simpler and easy to use. In addition, this model would be useful as a predictive tool for investigating the effect of various operating parameters on the transient flux decline profile during the start-up conditions in UF processes.

List of symbols

A	—	effective membrane area, m^2
a_1, a_2, a_3	—	parameter used in Eq. (19), dimensionless
C	—	concentration of PVA, kg/m^3
d_p	—	equivalent diameter of PVA, m
D	—	diffusivity of PVA, m^2/s
K	—	Boltzmann constant (1.38×10^{-23}), J/K
k	—	mass transfer coefficient, m/s
L	—	gel layer thickness, (m)
M_ω	—	molecular weight, kg/kg mol
N_{total}	—	total number of data points, dimensionless
Pe_w	—	water flux, dimensionless
Pe_w^0	—	pure water flux, dimensionless
R	—	radius of stirred cell, m
R_m	—	membrane hydraulic resistance, m^{-1}
R_g	—	gel layer resistance, m^{-1}
Re	—	Reynolds number at the bulk condition
Sc_b	—	Schmidt number at the bulk condition
Sh	—	Sherwood number at the bulk condition
T	—	absolute temperature, K
t	—	time of experiment, s
u	—	axial velocity, m/s
V	—	volume, m^3
V_w	—	radial average permeate flux, m^3/m^2 s
V_w^{exp}	—	experimental permeate flux, m^3/m^2 s

$V_{w,CF}^{ss}$ — steady state cross flow permeate flux, $m^3/m^2 s$
V_w^{cal} — calculated permeate flux, $m^3/m^2 s$
y — coordinate from the membrane, m
z — parameter in Eq. (13), $kg/kmol\,m^3$

Greek letters

v — parameter used in Eq. (5), dimensionless
α — specific gel layer resistance, m/kg
ω — angular speed of stirring, radian/s
μ — viscosity of the solution, Pa s
δ_c — thickness of concentration boundary layer, m
ε_g — gel porosity, dimensionless
ΔP — transmembrane pressure, kPa
ρ_g — gel density, kg/m^3
ρ — density, kg/m^3
τ_{total} — total operation time, dimensionless
τ — operation time, dimensionless

Subscript

0 — initial condition
b — bulk condition
p — permeate
f — feed
g — gel

Superscript

* — dimensionless

References

[1] G. Chen, C. Xijun, P.-L. Yue, M. Yongli, Treatment of textile desizing wastewater by pilot scale nanofiltration membrane separation, J. Membr. Sci. 127 (1997) 93–99.
[2] S.H. Lin, C.C. Lo, Fenton process for treatment of desizing wastewater, Water Res. 31 (1997) 2050–2056.
[3] S. Kim, T.H. Kim, C. Park, E.B. Shin, Electrochemical oxidation of polyvinyl alcohol using a RuO/Ti anode, Desalination 155 (2003) 49–57.
[4] Y. Chen, Z. Sun, Y. Yang, Q. Ke, Heterogeneous photocatalytic oxidation of polyvinyl alcohol in water, J. Photochem. Photobiol. A Chem. 142 (2001) 85–89.
[5] S.H. Lin, W.J. Lan, Polyvinyl alcohol recovery by ultrafiltration: Effects membrane type and operating conditions, Sep. Technol. 5 (1995) 97–103.
[6] J.J. Porter, Recovery of polyvinyl alcohol and hot water from the textile wastewater using thermally stable membranes, J. Membr. Sci. 151 (1998) 45–53.
[7] N.J. Saleh, A. Alhelaly, J.M. Ali, Q. Alsalhy, Recovery of PVA using polyethersulfone (pes) hollow fiber, ultrafiltration membranes: Part II: Effect of carboxymethyl, cellulose (CMC) concentration, Eng. & Tech. J. 27(5) (2009) 1008–1016.
[8] S.W. Lee, S.J. Haam, J.W. Kwak, J.H. Jang, Y.C. Lee, Ultrafiltration of desizing wastewater containing pva in Bench scale test, Environ. Technol. 20 (1999) 277–283.
[9] A. Sarkar, D. Sarkar, M. Gupta, C. Bhattacharjee, Recovery of Polyvinyl alcohol from desizing wastewater using a novel high-shear, ultrafiltration module, Clean—Soil, Air Water 40 (8) (2012) 830–837.
[10] S. Bhattacharjee, A. Sharma, P.K. Bhattacharya, A unified model for flux prediction during batch cell ultrafiltration, J. Membr. Sci. 111 (1996) 243–258.
[11] S.V. Satyanarayana, P.K. Bhattacharya, S. De, Flux decline during ultrafiltration of kraft black liquor using different flow modules: A comparative study, Sep. Purif. Technol. 20 (2000) 155–167.
[12] S. Chakraborty, B.C. Bag, S. DasGupta, J.K. Basu, S. De, Prediction of permeate flux and permeate concentration in nanofiltration of dye solution, Sep. Purif. Technol. 35 (2004) 141–152.
[13] C.W. van Oers, M.A.G. Vorstman, W.G.H.M. MulJselaar, P.A. J.M. Kerkhof, Unsteady-state flux behaviour in relation to the presence of a gel layer, J. Membr. Sci. 13 (1992) 231–246.
[14] J.S. Shen, R.F. Probstein, On the predictions of limiting flux in laminar ultrafiltration of macromolecular solutes, Ind. Eng. Chem. Fundam. 16 (1977) 459–465.
[15] D.R. Trettin, M.R. Doshi, Ultrafiltration in an unstirred batch cell, Ind. Eng. Chem. Fundam. 19 (1980) 189–194.
[16] M.W. Chudacek, A.G. Fane, The dynamics of polarization in unstirred and stirred ultrafiltration, J. Membr. Sci. 21 (1984) 145–160.
[17] W.F. Blatt, A. Dravid, A.S. Michaels, L. Nelson, Solute polarization and cake formation in membrane ultra-filtration: Causes, consequences and control techniques, In: J.E. Flinn (Ed.), Membrane Science and Technology, Plenum Press, New York, NY, 1970, pp. 47–57.
[18] P. Sharma, B. Sarkar, Prediction of permeate flux during ultrafiltration of polysaccharide in a stirred batch cell. Food Bioprocess Tech., doi: 10.1007/s11947-012-0990-7
[19] M.K. Purkait, S. DasGupta, S. De, Resistance in series model for micellar enhanced ultrafiltration of eosin dye, J. Colloid Interface Sci. 270 (2004) 496–506.
[20] L. Stryer, Biochemistry, Freeman, NewYork, NY, 1998.
[21] M. Cheryan, Ultrafiltration and microfiltration handbook, Technomic, Lancaster, PA, 1998. pp. 83–85.
[22] F. Belluci, E. Drioli, U. Scardi, Protein ultrafiltration: An experimental study, J. Appl. Polym. Sci. 19 (1975) 1639–1647.
[23] S. De, P.K. Bhattacharya, Modeling of ultrafiltration process for a two-component aqueous solution of low and high (gel-forming) molecular weight solutes, J. Membr. Sci. 136 (1997) 57–69.
[24] B. Sarkar, S. DasGupta, S. De, Effect of electric field during gel-layer controlled ultrafiltration of synthetic and fruit juice, J. Membr. Sci. 307 (2008) 268–276.
[25] S. Banerjee, S. De, An analytical solution of Sherwood number in a stirred continuous cell during steady state ultrafiltration, J. Membr. Sci. 389 (2012) 188–196.

Appendix

Viscosity: Viscosity of various PVA solutions at pH 7.0 and at 25°C is experimentally measured and can be expressed by the following polynomial (correlation coefficient 0.998) as follows:

$$\mu = 0.9(1 + 6.3 \times 10^{-2}C + 9.41 \times 10^{-3}C^2 + 4.45 \times 10^{-5}C^3) \times 10^{-3}. \quad (A1)$$

where μ is in Pa s and C is in kg/m^3.

Density: Density of PVA solution has been taken as $1{,}000\,kg/m^3$. The average gal layer density of PVA is taken to be $1{,}500\,kg/m^3$ [25].

Diffusivity: Diffusivity of PVA solution at feed concentration of 1, 3, 5, and $8\,kg/m^3$ are calculated using Eq. (12) and are found to be $7.7 \times 10^{-11}\,m^2/s$, $6.5 \times 10^{-11}\,m^2/s$, $5.35 \times 10^{-11}\,m^2/s$, and $4.4 \times 10^{-11}\,m^2/s$, respectively.